I&EC research
Industrial & Engineering Chemistry Research

pubs.acs.org/IECR

Article

Hybrid Micrometer Seed-Assisted Synthesis of Submicron Rectangular SAPO-34/18 Intergrowth Zeolites with Enhanced Methanol-to-Olefin Conversion

Chengguang Yang, Dong Fang, Xing Yu,* Meng Lyu, Xianni Bu, Hao Wang, Xinnan Lu, Yida Zhou, Shutao Xu,* and Peng Gao*

Cite This: *Ind. Eng. Chem. Res.* 2025, 64, 9951−9959

Read Online

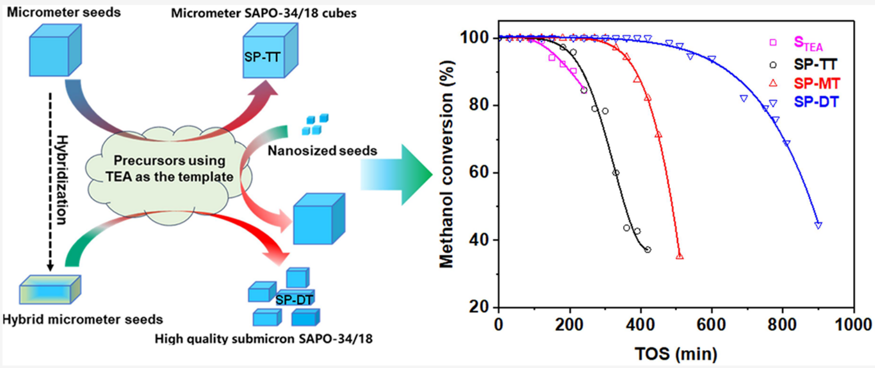

ABSTRACT: Efficient synthesis of SAPO-34/18 zeolites with relatively small crystal sizes has hitherto been difficult to achieve without expensive templates, abundant nanosized seeds, or additional crystal growth inhibitors for industrial MTO. Herein, we present a cost-effective and eco-friendly synthetic approach for submicrometer SAPO-34/18 intergrowth zeolites using triethylamine as the template with the assistance of hybrid micrometer seeds. In this work, the micrometer seeds, originally synthesized using triethylamine as the template, were hybridized with a precursor containing dimethylamine under hydrothermal conditions. The resultant SAPO-34/18 intergrowth zeolite exhibits a rectangular morphology and a reduced crystal size of approximately 700 nm. MAS NMR experiments show that as-synthesized SAPO-34/18 intergrowth zeolites with triethylamine as the sole template contained more Si(4Al) and Si(3Al) species. It is found that the ***d6r*** units in the hybrid seeds significantly improved nucleation, atom distribution, and etching resistance of SAPO-34/18 products. In addition, the submicrometer SAPO-34/18 intergrowth catalyst exhibited a 3-fold increased catalyst life and improved selectivity (88.3%) for light olefins in the MTO reaction. Therefore, the combination of efficient synthesis and good catalytic performance enables sustainable industrial synthesis of SAPO-34/18 intergrowth zeolites with reduced crystal size.

■ INTRODUCTION

Zeolites are widely used as heterogeneous catalysts in various industrial processes due to their molecular shape selectivity, suitable acidity, large surface areas, and high hydrothermal stability.[1−10] SAPO-34 zeolite is widely used and studied as a shape-selective catalyst for methanol-to-olefin (MTO) conversion, owing to its unique pore structures and Brønsted acid sites (BAS) with moderate acid strength.[11,12] Recently, a number of patents have justified the good performance of CHA/AEI intergrowth materials in the MTO process.[13] However, the microporous SAPO-34/18 crystal suffers from rapid deactivation due to diffusion limitations.[14,15] Decreasing the crystal size is considered an effective strategy for prolonging catalyst life. However, fewer cases have been reported on SAPO-34/18 in this aspect compared to SAPO-34. Although significant progress has been made in synthetic strategies such as microwave-assisted synthesis,[16] dry gel conversion,[17−19] ultrasound-assisted syntheses,[20] and fast high-temperature synthesis,[21] these methodologies remain primarily confined to the laboratory scale.[22] Generally, the synthesis of SAPO-34 featuring small crystal sizes requires expensive tetraethylammonium hydroxide (TEAOH) as the template. To decrease production costs, amines, such as triethylamine (TEA), diethylamine (DEA), and morpholine

Received: January 25, 2025
Revised: April 17, 2025
Accepted: April 23, 2025
Published: May 7, 2025

https://doi.org/10.1021/acs.iecr.5c00386
Ind. Eng. Chem. Res. 2025, 64, 9951−9959

Scheme 1. Schematic Diagram for the Synthesis of Submicron-Sized SAPO-34/18 Intergrowth Zeolites with the Assistance of Hybrid Seeds

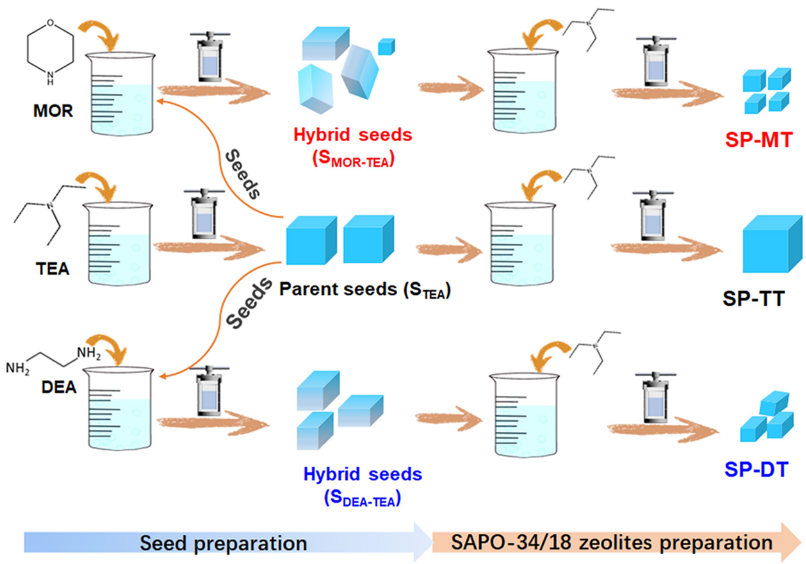

(MOR), have been explored as cotemplates. Among the four templates, TEA stands out due to its facile availability from ethanol through vapor-phase catalysis at atmospheric pressure and high production capacity. Given the structural similarities between SAPO-18 and SAPO-34, it is easy to form intergrowth structures using TEA as the sole template. However, SAPO-34/18 intergrowth zeolites prepared using TEA as the template normally exhibit a relatively large crystal size.[23−26] Liu et al.[27] found that SAPO-34 prepared using TEA as the template exhibited the smallest crystal size (around 2 μm) and the lowest crystallinity, whereas MOR as the template led to the largest crystals of approximately 10 μm. Additionally, SAPO-34 synthesized with DEA as the template showed the highest crystallinity. Masoumi et al. successfully synthesized nanosized SAPO-34 (around 640 nm) using a mixed template comprising 25% MOR, 25% TEA, and 50% TEAOH.[28] Carreon et al. synthesized submicron SAPO-34 in the presence of crystal growth inhibitors (CGIs).[29] Yu and co-workers prepared SAPO-34 (700−800 nm) by adding nanosized seeds into the initial gel with TEA as the template.[30,31] Liu and co-workers prepared nanosized SAPO-34 (50−350 nm) through a postsynthesis milling and recrystallization method.[32] Despite substantial progress, it remains a significant challenge to synthesize SAPO-34/18 intergrowth zeolites with reduced crystal size in the absence of nanoscale seeds, CGIs, or TEAOH.

Previous studies have confirmed that the type of template significantly impacts the phase, acidity, crystallinity, and crystal size. Liu et al.[27] displayed that silicon incorporation into the framework follows the trend of SAPO-34 (TEA) < SAPO-34 (MOR) < SAPO-34 (DEA), due to template molecular size, with higher Si(4Al) contents in SAPO-34 (MOR) and SAPO-34 (DEA). Nakhaei Pour and co-workers[33] found that template mixtures affected the crystal size, with SAPO-34 (TEA/DEA) < SAPO-34 (TEA) < SAPO-34 (DEA), and Si content decreasing in the same order. In addition, Tian and co-workers highlighted the importance of double 6-ring (***d6r***) and Si−O−Al domains for qualified SAPO-type seeds.[34] Considering China's total olefin production capacity exceeding 16 Mt/a,[35] cost-effective and environmentally sustainable methods for the synthesis of SAPO-34/18 zeolites with small crystal size and good catalytic performance are very desirable for large-scale MTO applications.

Inspired by these synthesis advancements of zeolites driven by the development of MTO industrialization processes, we designed a facile, cost-effective, and eco-friendly route for the synthesis of submicrometer SAPO-34/18 intergrowth zeolite by adding hybrid seeds. These seeds, resulting from hybridizing parent seeds with a precursor using DEA as the template, contain abundant ***d6r*** units. It is speculated that the content of ***d6r*** units played an important role in determining both the nucleation and morphology. Moreover, a low synthetic temperature (165 °C) favors nucleation while inhibiting crystal growth, yielding rectangular SAPO-34/18 intergrowth zeolite with a crystal size of ∼700 nm, higher acid concentration and strength, and a rich Si(4Al) coordination environment. Owing to these advantages, the resultant SAPO-34/18 catalyst exhibits a 3-fold longer lifetime and higher selectivity for light olefins (up to 88.3%). These results pave the way for an efficient and large-scale production of high-quality silicoaluminophosphate (SAPO) materials.

■ RESULTS AND DISCUSSION

Synthesis of Submicron SAPO-34/18 Intergrowth Zeolites. Scheme 1 outlines a concise synthetic procedure for preparing submicrometer SAPO-34/18 intergrowth zeolites using hybrid seeds. The process includes the synthesis of the parent seeds and hybrid seeds and the subsequent synthesis of final SAPO-34/18 products. The parent seeds denoted as S_{TEA} were synthesized by using TEA as the template. Then, the hybrid seeds, designated as $S_{DEA-TEA}$, were prepared by hybridization of S_{TEA} with the precursor using DEA as the template. Similarly, $S_{MOR-TEA}$ was also obtained by the hydrothermal treatment of S_{TEA} with a precursor using MOR as the template. Finally, conventional SAPO-34/18 (denoted as SP-TT) was synthesized by introducing S_{TEA} into the precursor with TEA as the template. It is worth noting that the submicrometer SAPO-34/18 (designated as SP-DT) with a rectangular morphology was synthesized from the same precursor but with the substitution of $S_{DEA-TEA}$ for S_{TEA}.

https://doi.org/10.1021/acs.iecr.5c00386
Ind. Eng. Chem. Res. 2025, 64, 9951−9959

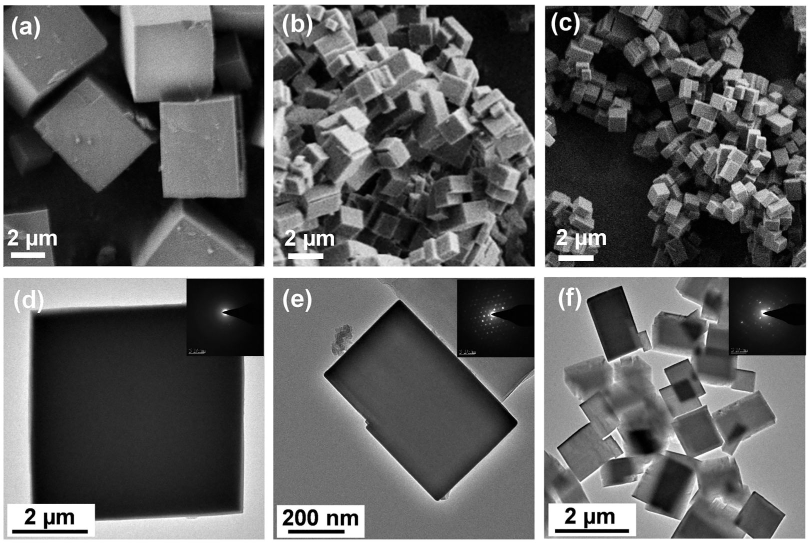

Figure 1. (a−c) SEM and (d−f) TEM images of (a, d) SP-TT, (b, e) SP-DT, and (c, f) SP-MT samples.

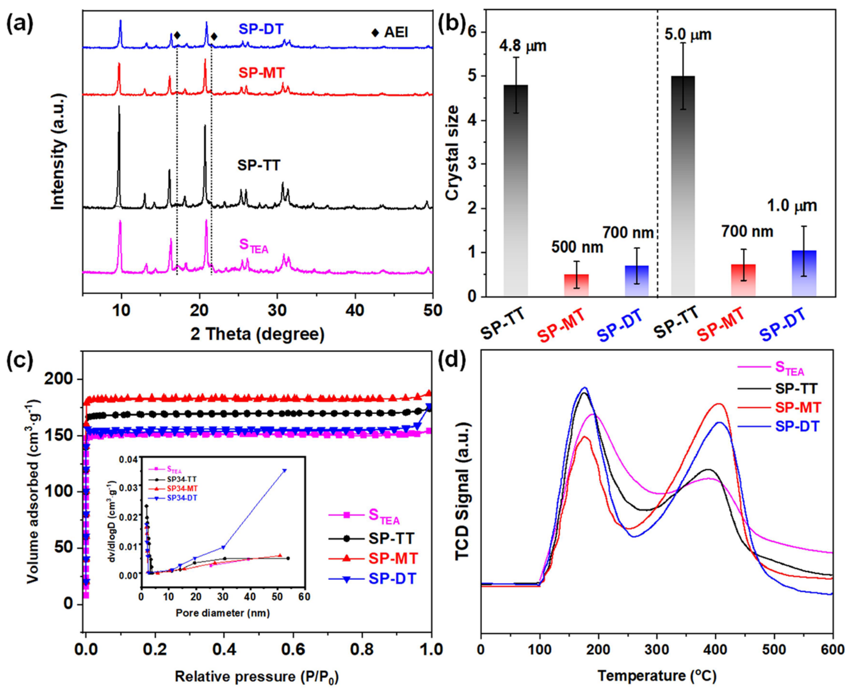

Figure 2. (a) XRD patterns, (b) average shortest edge size (left) and the average crystal size, (c) N_2 adsorption−desorption isotherms, the inset is BJH pore size distribution, and (d) NH_3-TPD profiles of S_{TEA}, SP-TT, SP-MT, and SP34-DT samples.

Similarly, another submicrometer SP-MT was synthesized from the same precursor with the assistance of $S_{MOR\text{-}TEA}$. Figures S1 and 2a present XRD patterns of as-synthesized micrometer seeds. S_{TEA} exhibited the typical characteristic diffraction peaks at 9.6°, 14.2°, 16.2°, 20.8°, 26.0°, and 31.1°, corresponding to the CHA topology (as referenced to the standard JCPDS 47-0439). Besides, additional peaks at 17.0° and 21.2° were observed on S_{TEA}, which can be ascribed to the AEI topology structure. According to the peak intensity, S_{TEA} primarily consists of SAPO-34. Meanwhile, S_{TEA} presents a surface area of 501 m^2 g^{-1} and a micropore volume of 0.26 cm^3 g^{-1} (Table S1). XRD patterns of $S_{DEA\text{-}TEA}$ and $S_{MOR\text{-}TEA}$ match well with those simulated from the CHA framework type, indicating the successful synthesis of the pure SAPO-34 phase via the hybridization process. Figure S2a−c shows the SEM images of the three seeds. It can be clearly found that S_{TEA} showed a cubic morphology with a crystal size of 2 μm. However, obvious differences in the morphology and crystal size were observed for S_{TEA} and the hybrid seeds. The hybrid seeds $S_{DEA\text{-}TEA}$ and $S_{MOR\text{-}TEA}$ displayed a rectangular morphology with an average thickness of approximately 2 μm and crystal sizes ranging from 1 to 5 μm. These results suggest that the hybridization process has a significant impact on the physicochemical properties, compared with parent seeds. EDX elemental mapping measurements were performed on S_{TEA}, $S_{DEA\text{-}TEA}$, and $S_{MOR\text{-}TEA}$. As shown in Figures S3−S5, the Si, Al, and P atoms are homogeneously distributed in all the samples. The molar Si/Al/P ratios of S_{TEA}, $S_{DEA\text{-}TEA}$, and $S_{MOR\text{-}TEA}$ are $Si_{0.10}Al_{0.50}P_{0.40}$, $Si_{0.10}Al_{0.50}P_{0.40}$, and $Si_{0.107}Al_{0.526}P_{0.377}$ (Table S2), respectively. Furthermore, the XRF analysis revealed the

https://doi.org/10.1021/acs.iecr.5c00386
Ind. Eng. Chem. Res. 2025, 64, 9951−9959

Table 1. Textural Properties of As-Synthesized SAPO-34/18 Intergrowth Zeolites

sample	elemental compositions (mol %)		S_{total}[a] (m^2 g^{-1})	S_{micro}[b] (m^2 g^{-1})	V_{total}[c] (cm^3 g^{-1})	V_{micro}[d] (cm^3 g^{-1})	AEI phase content/%[e]
	XRF	XPS					
SP-TT	$Si_{0.067}Al_{0.491}P_{0.442}$	$Si_{0.173}Al_{0.462}P_{0.364}$	511	497	0.27	0.26	1%
SP-MT	$Si_{0.067}Al_{0.491}P_{0.442}$	$Si_{0.210}Al_{0.428}P_{0.362}$	548	540	0.29	0.28	4%
SP-DT	$Si_{0.067}Al_{0.491}P_{0.442}$	$Si_{0.241}Al_{0.416}P_{0.343}$	467	458	0.27	0.24	5%
SP-TT-H	$Si_{0.063}Al_{0.491}P_{0.446}$	$Si_{0.175}Al_{0.440}P_{0.380}$	472	461	0.25	0.24	1%
SP-MT-H	$Si_{0.058}Al_{0.496}P_{0.446}$	$Si_{0.224}Al_{0.408}P_{0.368}$	503	493	0.27	0.26	2%
SP-DT-H	$Si_{0.062}Al_{0.496}P_{0.442}$	$Si_{0.219}Al_{0.411}P_{0.370}$	434	423	0.24	0.22	3%

[a]BET surface area. [b]t-plot micropore surface area. [c]t-plot total pore volume. [d]t-plot micropore volume. [e]Determined by HighScore Plus.

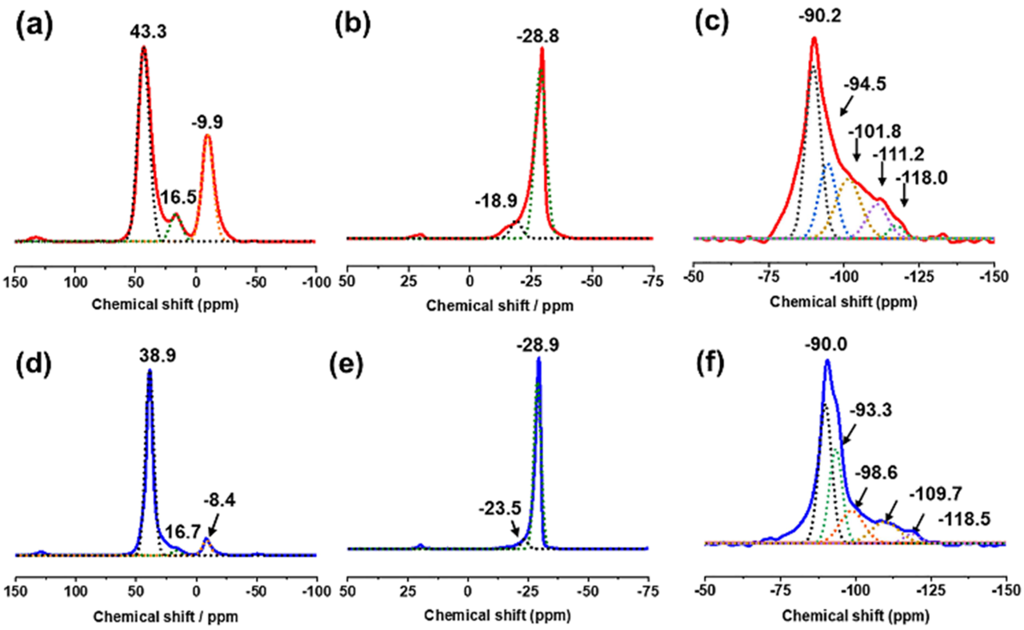

Figure 3. ^{27}Al, ^{31}P, and ^{29}Si MAS NMR spectra of (a−c) SP-TT and (d−f) SP-DT samples.

bulk compositions to be $Si_{0.076}Al_{0.384}P_{0.540}$, $Si_{0.076}Al_{0.384}P_{0.540}$, and $Si_{0.072}Al_{0.372}P_{0.556}$, respectively. Upon these results, it is evident that the surface Si and Al contents (calculated as Si/(Si + Al + P) and Al/(Si + Al + P) from the EDS analysis) are higher than their corresponding bulk compositions as determined by the XRF analysis. This suggests that the surfaces of the products are enriched in Si and Al elements compared to their bulk compositions.

Figures 1, 2b, and S6 present the morphology and crystal size distribution of the corresponding SAPO-34/18 intergrowth zeolites. With the assistance of hybrid seeds, the resultant SP-DT and SP-MT crystals exhibit rectangular morphologies. The shortest edges of SP-DT and SP-MT are centered at 500 and 700 nm, and the average overall crystal sizes are 1.0 μm and 700 nm, respectively. Conversely, SP-TT using S_{TEA} as the seed features larger cubic crystals with a size of approximately 4.8 μm. Figure 1d−f shows the TEM images of the three SAPO-34 crystals. Notably, no diffraction spots are observed for SP-TT due to a relatively large crystal size. In contrast, the SP-DT and SP-MT samples generated uniform diffraction spots. For comparison, the sample synthesized in the absence of any seeds at 165 °C possesses low relative crystallinity, owing to the formation of amorphous solids (Figure S7). Furthermore, when prepared using TEA as a template in the presence of nanosized seeds (S_{TEAOH}), the sample exhibits a small crystal size of approximately 2 μm (Figures S8 and S9). The yield of SAPO-34/18 obtained by this method is 10.8%, calculated based on the precursor weight. Interestingly, the use of hybrid seeds of equal mass results in a product yield of 16.0%. These results indicate that the type of seeds appears to play a crucial role in nucleation rather than crystal growth under low seed consumption and relatively low synthesis temperature.

As shown in Figure 2a, all the products exhibit typical diffraction peaks at 9.6°, 12.9°, 16.2°, 20.8°, 26.0°, and 31.1°, corresponding to the CHA topology. Further, additional peaks at 17.0° and 21.2° indicate that all the products are AEI/CHA intergrowth zeolites but with CHA as a dominant phase. The content of the AEI phase, as determined by HighScore Plus, is less than 5%. Compared to SP-TT, lower peak intensities are observed for the SP-DT and SP-MT samples, suggesting that their crystal sizes and ordering degrees are different. In addition, pure SAPO-34 (Figure S10) can be synthesized by increasing the seed content (8%, based on Al_2O_3). N_2 physisorption experiments were carried out to study the textural properties of the products (Figure 2c). It can be found that all samples exhibit type-I absorption−desorption isotherms.[36] The sudden uptake at $P/P_0 < 0.01$ can be attributed to the micropore filling. Notably, no uptake at the pressure range of $0.95 < P/P_0 < 1.0$ is observed for SP-TT, which suggests the absence of macropores in SP-TT. Additionally, both the microporous area and volume tend to decrease in the order of SP-MT > SP-TT > SP-DT. The microporous area and volume of SP-DT are 467 m^2 g^{-1} and 0.27 cm^3 g^{-1},

https://doi.org/10.1021/acs.iecr.5c00386
Ind. Eng. Chem. Res. 2025, 64, 9951−9959

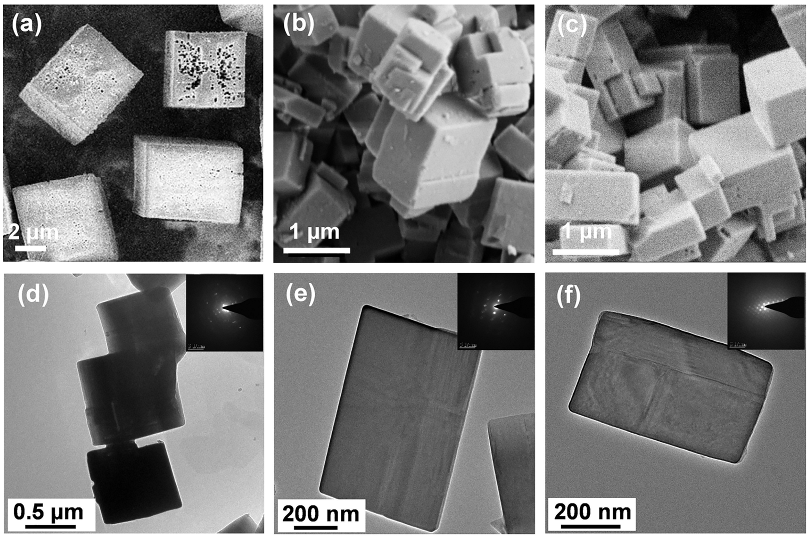

Figure 4. SEM images (a−c) and TEM images (d−f) of (a, d) SP-TT-H, (b, e) SP-DT-H, and (c, f) SP-MT-H samples.

respectively. The microporous area and volume of SP-DT are 548 m^2 g^{-1} and 0.29 cm^3 g^{-1}, respectively (Table 1). SP-MT shows the largest surface area and micropore volume, probably corresponding to the smallest crystal size. XRF results indicate that all samples have the same bulk element composition of $Si_{0.067}Al_{0.491}P_{0.442}$. The surface element compositions determined by XPS are $Si_{0.173}Al_{0.462}P_{0.364}$, $Si_{0.210}Al_{0.428}P_{0.362}$, and $Si_{0.241}Al_{0.416}P_{0.343}$ for SP-TT, SP-MT, and SP-DT, respectively, suggesting an enrichment of Si on their surfaces compared to their bulk composition. NH_3-TPD profiles (Figure 2d) show that S_{TEA} presents two desorption peaks centered at 191 and 384 °C, which can be ascribed to weak and strong acid sites.[37] The obtained SP-TT possesses two desorption peaks centered at 175 and 387 °C, respectively, indicating a decrease in strength in weak acid sites. In comparison, the desorption peaks for SP-MT and SP-DT are centered at 175 and 405 °C, respectively, which indicates similar strengths for the weak acid sites and relatively higher strengths for the strong acid sites. Furthermore, SP-MT exhibits the greatest proportion of strong acid sites, accompanied by a moderate proportion of weak acid sites.

The ^{27}Al, ^{31}P, and ^{29}Si MAS NMR technique was employed to study the chemical coordination environment of constituent atoms in as-synthesized SP-DT and conventional SP-TT. As shown in Figure 3a,d, the multipeak fitting exhibits prominent signals at 43.3 and 38.9 ppm, which can be ascribed to the tetrahedral Al atoms within the framework.[38,39] In addition, peaks observed at 16.5 and 16.7 ppm are assigned to the 5-coordinated Al atoms, arising from the combination of tetrahedrally coordinated Al species with a single water molecule. The peaks at −9.9 ppm and −8.4 ppm correspond to 6-coordinated Al species, resulting from the interaction of 4-coordinated framework Al atoms with two water molecules or extra-framework Al species. Notably, SP-DT exhibits fewer 5-coordinated and octahedrally Al species compared with SP-TT, potentially due to a reduced number of framework defects. The ^{31}P MAS NMR spectrum (Figure 3b,e) contains a strong peak at around −28.8 ppm, which is attributed to the P(Al) species.[40] Moreover, the intensity of partially hydrated P(OAl)x(H_2O)y species of SP-DT is lower than that of SP-TT, with chemical shifts of −18.9 and −23.5 ppm, indicating that fewer defects exist in SP-DT. The ^{29}Si MAS NMR spectrum (Figure 3c) shows that SP-TT contains a strong signal at −90.2 ppm corresponding to Si(4Al) species, with additional peaks at −94.5, −101.8, −111.2, and −118.0 ppm, corresponding to Si(3Al), Si(2Al), Si(1Al), and Si(0Al) species, respectively.[41] These peaks shift to −90.0, −93.3, −98.6, 109.7, and −118.5 ppm for SP-DT (Figure 3f). According to the NMR analysis, Si atoms are predominantly present as Si(4Al) and Si(3Al) species in SP-DT, in contrast to Si(2Al), Si(1Al), and Si(0Al) species. This suggests that a tunable Si distribution was achieved for submicron SP-DT with the aid of hybrid seeds.

Proposed Crystallization Mechanism. Acid etching was performed on SP-TT, SP-DT, and SP-MT to study the effect of seeds on the framework atom distribution.[42] It is well-known that the framework Al species are sensitive, whereas Si species exhibit relatively high stability during the postsynthesis treatment process. As shown in Figure 4a−c, the surface of SP-TT-H exhibits an X-type or a butterfly-like defect. Previous studies indicate that SAPO-34 cubes synthesized using TEA as the template initially grow along a specific direction, forming a crystal with eight pyramids and a central void that fills to form a perfect cube.[36,43] The X-type portions are less stable and preferentially etched, leading to a butterfly-like defect after acid treatment. In contrast, no surface defects are observed on SP-DT-H and SP-MT-H, further confirming distinct element distributions in the three samples. TEM images (Figure 4d−f) also show that SP-DT-H and SP-MT-H possess smooth surfaces with smaller crystal sizes, whereas X-type defects are not observed on the selected SP-TT-H with the smallest particle size due to the relatively large crystal sizes.

Additionally, after postsynthesis treatment with a HNO_3 solution, all the samples retain the original CHA/AEI topology structure; however, a significant decrease is observed in the peak intensities at 12.8°, 16.2°, and 20.7°, corresponding to the (110), (021), and (211) crystal planes (Figure S11). Unlike SP-DT-H, SP-TT-H and SP-MT-H exhibit increased peak intensity at 9.6°, ascribing to the (101) crystal plane. The overall and (101) plane relative crystallinities were also calculated. As displayed in Table S3, the overall relative crystallinities of SP-TT, SP-DT, and SP-MT are 100, 34.0, and 42.1%, respectively. After acid etching treatment, the overall crystallinities of SP-TT-H, SP-DT-H, and SP-MT-H are 67.2,

https://doi.org/10.1021/acs.iecr.5c00386
Ind. Eng. Chem. Res. 2025, 64, 9951−9959

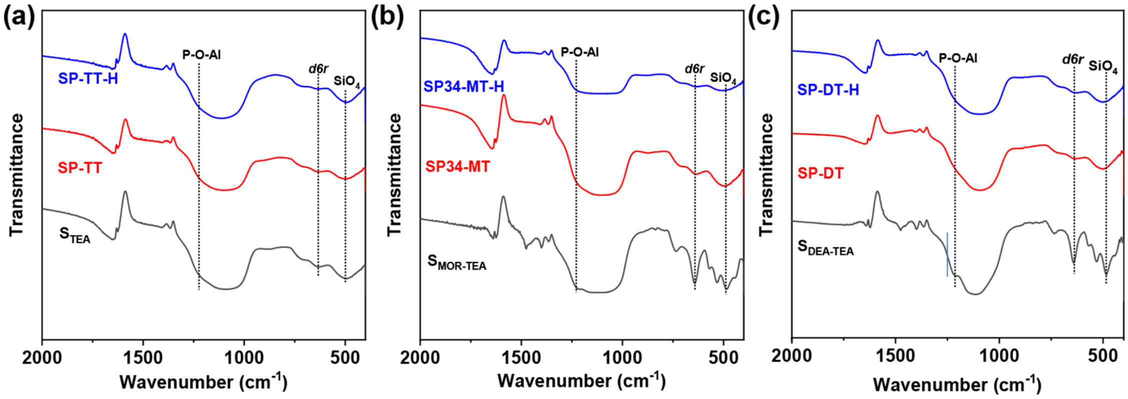

Figure 5. FT-IR spectra of (a) S_{TEA}, SP-TT, and SP-TT-H, (b) $S_{MOR-TEA}$, SP34-MT, and SP-MT-H, and (c) $S_{DEA-TEA}$, SP34-DT, and SP-DT-H.

Scheme 2. Proposed Synthetic Mechanism of (a) SP-TT and (b) SP-DT Prepared through the Seed-Assisted Synthesis Method

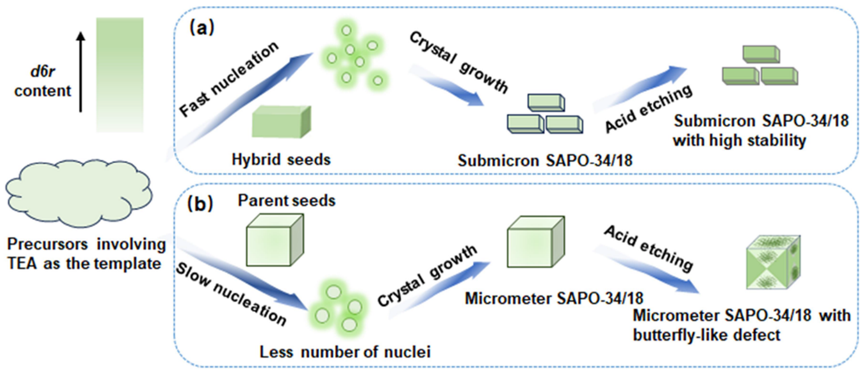

26.0, and 23.7%, respectively (Table S3). In addition, the relative crystallinities of the (101) plane of SP-TT-H, SP-DT-H, and SP-MT-H change from 100, 34.4, and 38%, respectively, into 104.8, 27.8, and 39.2%, respectively (Table S3). The acid etching treatment decreases overall crystallinities, except for the (101) crystal plane. SP-DT-H and SP-MT-H display the type-I isotherms with no significant changes at $P/P_0 < 0.01$ compared with corresponding SP-DT and SP-MT, indicating that microporous structures remain dominant (Figure S12).[36] All of the samples before and after acid treatment show a broad pore size distribution ranging from 10 to 55 nm, which may be ascribed to particle accumulation. The bulk compositions of SP-TT-H, SP-MT-H, and SP-DT-H determined by the XRF analysis are $Si_{0.063}Al_{0.491}P_{0.446}$, $Si_{0.058}Al_{0.496}P_{0.446}$, and $Si_{0.062}Al_{0.496}P_{0.422}$, respectively (Table 1). MAS NMR spectra indicate that the content of 6-coordinated Al species in SP-TT-H (Figure S13a) is lower than in SP-DT-H, and $Si(OAl)_n(OH)_{4-n}$ species at −81.6 ppm, originating from the Si−OH−Al bond fracture, are absent in SP-DT-H. In addition, the contents of Si(4Al) and Si(3Al) species decrease along with a signal at −90.2 ppm for SP-TT-H. The amounts of $P(OAl)_4(H_2O)_y$ (y = 1 or 2) species increase with increasing Al leaching (Figure S13b,e). NH_3-TPD profiles in Figure S14 reveal a decrease in both the contents of acid sites and the strength of strong acids for SP-TT-H and SP-DT-H, resulting in a loss of active sites. Notably, SP-MT-H retains most of its acid sites, probably contributing to the stable lifespan of the MTO reaction.

Furthermore, Figure 5 shows FT-IR spectra of seeds, as-synthesized SAPO-34/18 zeolites, and acid-treated SAPO-34/18 zeolites. All of the samples exhibit a clear band at 640 cm^{-1}, which is attributed to the adsorption of ***d6r*** units. Other bands at 1220, 1082, 724, and 484 cm^{-1} are in turn attributed to the absorption of P−O−Al, O−P(Al)-O, P(Al)-O, and SiO_4.[43] An increasing tendency could be observed in hybrid seeds compared to S_{TEA} when comparing the relative band intensity (I_{640}/I_{1220}) for the bands centered at 640 cm^{-1} (corresponding to the absorption of ***d6r*** units) and 1220 cm^{-1} (corresponding to the absorption of P−O−Al). Obviously, $S_{TEA-MOR}$ and $S_{TEA-DEA}$ exhibit a more concentrated distribution of ***d6r*** units compared with S_{TEA}. The resultant SP-TT, SP-DT, and SP-MT have a similar band intensity at 640 cm^{-1}. It is speculated that $S_{TEA-MOR}$ and $S_{TEA-DEA}$ (Figure S15) retained abundant ***d6r*** units after dissolution, thereby accelerating nucleation over the crystallization of SAPO-34/18 at a relatively low temperature.[34]

Consequently, a synthetic mechanism is proposed in Scheme 2. Specifically, in the initial gel containing the TEA template, the incorporation of hybrid seeds rich in ***d6r*** units (Figure 5) can promote the formation of nuclei, which subsequently grow into rectangular submicrometer SAPO-34/18 intergrowth zeolite comprising a higher proportion of Si(4Al) and Si(3Al) species. Even during the subsequent acid treatment process, most Si(4Al) and Si(3Al) species and the rectangular morphology were preserved, which suggests the high stability of the zeolitic framework of the as-prepared SAPO-34/18 intergrowth zeolite. Conversely, the introduction of SAPO-34/18 cubic seeds with fewer ***d6r*** units resulted in micrometer-sized SP-TT cubes. Furthermore, the distribution of framework atoms plays a key role in the material's sensitivity to HNO_3.

https://doi.org/10.1021/acs.iecr.5c00386
Ind. Eng. Chem. Res. 2025, 64, 9951−9959

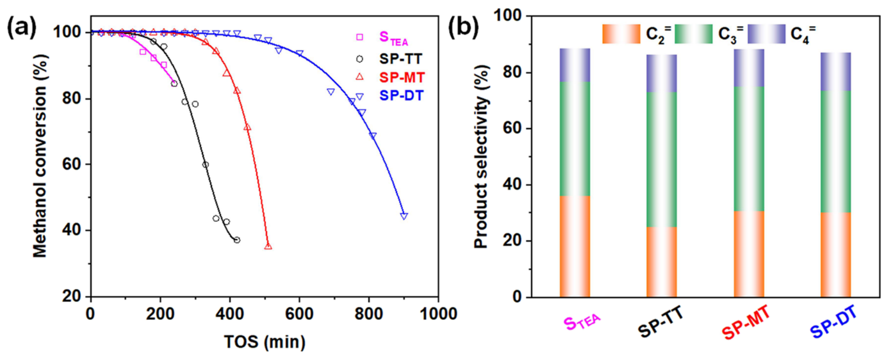

Figure 6. (a) Methanol conversion as a function of time on stream and (b) product selectivity over S_{TEA}, SP-TT, SP-DT, and SP-MT catalysts. The values were taken as TOS = 2 h. Reaction conditions: T = 400 °C, P = 1 atm, and WHSV = 1.0 h^{-1}.

Catalytic Performance in the MTO Reaction. Methanol conversion over as-synthesized submicrometer SAPO-34/18 zeolites was evaluated in a fixed-bed reactor. Figure 6 presents the product selectivity and catalytic lifetimes of S_{TEA}, SP-TT, SP-DT, and SP-MT. The parent seed S_{TEA} shows a catalyst life of 120 min with over 95% methanol conversion. The selectivities for $C_2^=-C_4^=$ and $C_2^=+C_3^=$ are 88.3 and 76.7%, respectively, and the $C_2^=$ selectivity is 36.0%. Notably, SP-DT and SP-MT show significantly prolonged catalyst lifespans compared with SP-TT. Among the three catalysts, SP-DT possesses the longest lifespan of 510 min, which is three times greater than that of SP-TT (180 min) and surpasses that of SP-MT (330 min). It is found that the selectivities for $C_2^=-C_4^=$ observed on SP-MT and SP-DT are 88.3 and 87.1% (TOS = 2 h), respectively, and the selectivities for $C_2^=+C_3^=$ are 75.1 and 73.6%, respectively (Table S4). Conversely, SP-TT exhibits the lowest selectivities for $C_2^=-C_4^=$ (86.2%) and $C_2^=+C_3^=$ (73.0%). Furthermore, the selectivities for $C_2^=$ over SP-DT and SP-MT reach 30.6% and 30.0%, respectively, representing an approximately 6% increase compared to that of SP-TT (24.8%).[44−46] In addition, the resultant SP-DT exhibits a prolonged catalyst lifetime under the same reaction conditions, outperforming most of previously reported SAPO-34 with TEA as a template (Table S5).[42,47−52] After postsynthesis treatment, the selectivity for $C_2^=$ with SP-DT-H increases to 34.1%, leading to an increase in $C_2^=+C_3^=$ selectivity (89.9%). As shown in Figure S16, SP-DT-H exhibits a lifetime of 420 min, 3.5 times that of SP-TT-H (120 min), surpassing SP-MT-H (360 min). Therefore, the degradation of the CHA framework, accompanied by reduced crystallinity (Figures 2a and S11), pore volume (Table 1), and acidity (Figure S13), leads to unimproved catalytic performance.

As shown in Figure S17, TG curves within the temperature range of 400 and 700 °C reveal that the spent SP-TT exhibits a weight loss of 14%. Compared with the spent SP-TT, the deactivated SP-DT and SP-MT show a higher weight loss of around 20.0%. The enhanced coke capacity can be attributed to the decreased crystal sizes (Figure 1) and increased strong acid sites (Figure 2d) of the submicrometer SAPO-34/18 zeolites. In addition, the average coking rates (R_{Coke}) for SP-TT, SP-MT, and SP-MT (Table S6) are 0.81, 0.61, and 0.38 mg·min^{-1}, respectively. The methanol consumption for coke formation (P_{Coke}) of SP-TT, SP-DT, and SP-MT was also calculated, with values of 0.05 g·g_{MeOH}^{-1}, 0.02 g·g_{MeOH}^{-1}, and 0.04 g·g_{MeOH}^{-1}, respectively. SP-TT demonstrates a higher proportion of methanol consumption for coke formation compared with SP-DT and SP-MT. The highest strong acid density of SP-MT caused its fast deactivation, showing relatively poor stability compared to SP-DT, although it displays the smallest crystal sizes with the highest surface area and micropore volume. Therefore, due to the reduced crystal sizes and suitable acidity, SP-DT showed superior catalytic performance over SP-MT and SP-TT.

■ CONCLUSIONS

In summary, this work provides an innovative approach for the synthesis of submicrometer SAPO-34/18 intergrowth zeolites with the assistance of hybrid micrometer SAPO-34/18 seeds using TEA as the sole template. The hybrid seeds were prepared through in situ hydrothermal treatment of S_{TEA} with precursors containing a DEA or MOR template, which is a crucial step for the synthesis of submicron SAPO-34/18. The qualified hybrid seeds enriched with ***d6r*** units[34] might provide more nuclei after dissolution. The acceleration in nucleation favors the synthesis of relatively small SAPO-34/18 crystals at a low temperature of 165 °C. The as-synthesized SAPO-34/18 possesses moderate acidity and a reduced crystal size of 700 nm. Additionally, it contains more Si(4Al) and Si(3Al) species, which remain stable after acid etching. Due to the advantages of reduced crystal size, SP-DT and SP-MT demonstrated significantly prolonged catalyst lifetimes. Furthermore, higher selectivity for $C_2^=-C_4^=$ has been achieved on the two submicron SAPO-34/18 intergrowth zeolites. Therefore, this strategy offers a straightforward, cost-effective, and easily scalable route for producing potential submicrometer-sized SAPO-type zeolites with enhanced catalytic performance.

■ ASSOCIATED CONTENT

Supporting Information

The Supporting Information is available free of charge at https://pubs.acs.org/doi/10.1021/acs.iecr.5c00386.

Description of chemicals and materials, synthesis of parent seeds, hybrid seeds and corresponding conventional and submicron SAPO-34/18 intergrowth zeolite and their post synthesis treatment process, characterization, and testing of catalytic performance (PDF)

■ AUTHOR INFORMATION

Corresponding Authors

Xing Yu − *CAS Key Laboratory of Low-Carbon Conversion Science and Engineering, Shanghai Advanced Research Institute, Chinese Academy of Sciences, Shanghai 201210, P. R. China*; Email: yuxing@sari.ac.cn

Shutao Xu – *National Engineering Research Center of Lower-Carbon Catalysis Technology, Dalian Institute of Chemical Physics, Chinese Academy of Sciences, Dalian 116023, P. R. China;* orcid.org/0000-0003-4722-8371; Email: xushutao@dicp.ac.cn

Peng Gao – *CAS Key Laboratory of Low-Carbon Conversion Science and Engineering, Shanghai Advanced Research Institute, Chinese Academy of Sciences, Shanghai 201210, P. R. China; University of Chinese Academy of Sciences, Beijing 100049, P. R. China;* orcid.org/0000-0003-4859-4488; Phone: +86-021-20350994; Email: gaopeng@sari.ac.cn; Fax: +86-021-20608066

Authors

Chengguang Yang – *CAS Key Laboratory of Low-Carbon Conversion Science and Engineering, Shanghai Advanced Research Institute, Chinese Academy of Sciences, Shanghai 201210, P. R. China*

Dong Fang – *CAS Key Laboratory of Low-Carbon Conversion Science and Engineering, Shanghai Advanced Research Institute, Chinese Academy of Sciences, Shanghai 201210, P. R. China; University of Chinese Academy of Sciences, Beijing 100049, P. R. China*

Meng Lyu – *CAS Key Laboratory of Low-Carbon Conversion Science and Engineering, Shanghai Advanced Research Institute, Chinese Academy of Sciences, Shanghai 201210, P. R. China*

Xianni Bu – *CAS Key Laboratory of Low-Carbon Conversion Science and Engineering, Shanghai Advanced Research Institute, Chinese Academy of Sciences, Shanghai 201210, P. R. China*

Hao Wang – *CAS Key Laboratory of Low-Carbon Conversion Science and Engineering, Shanghai Advanced Research Institute, Chinese Academy of Sciences, Shanghai 201210, P. R. China;* orcid.org/0000-0002-9360-5150

Xinnan Lu – *CAS Key Laboratory of Low-Carbon Conversion Science and Engineering, Shanghai Advanced Research Institute, Chinese Academy of Sciences, Shanghai 201210, P. R. China*

Yida Zhou – *National Engineering Research Center of Lower-Carbon Catalysis Technology, Dalian Institute of Chemical Physics, Chinese Academy of Sciences, Dalian 116023, P. R. China*

Complete contact information is available at:
https://pubs.acs.org/10.1021/acs.iecr.5c00386

Author Contributions

The manuscript was written through contributions of all authors. All authors have given approval to the final version of the manuscript.

Notes

The authors declare no competing financial interest.

■ ACKNOWLEDGMENTS

We thank the National Natural Science Foundation of China (22293023, 22293022, 22172189, U22B20136, 22241801), Program of Shanghai Academic Research Leader (22XD1424100), Science and Technology Commission of Shanghai Municipality (23ZR1481700), CAS Youth Interdisciplinary Team, Chinese Academy of Sciences, Shanghai Branch (CASSHB-QNPD-2023-024), and Qinchuangyuan "Scientists + Engineers" Team Construction Program of Shanxi Province (2023KXJ-276) for supporting this work.

■ REFERENCES

(1) Yang, L.; Wang, C.; Zhang, L.; Dai, W.; Chu, Y.; Xu, J.; Wu, G.; Gao, M.; Liu, W.; Xu, Z.; Wang, P.; Guan, N.; Dyballa, M.; Ye, M.; Deng, F.; Fan, W.; Li, L. Stabilizing the framework of SAPO-34 zeolite toward long-term methanol-to-olefins conversion. *Nat. Commun.* **2021**, *12* (1), 4661.

(2) Chen, L. H.; Sun, M. H.; Wang, Z.; Yang, W.; Xie, Z.; Su, B. L. Hierarchically Structured Zeolites: From Design to Application. *Chem. Rev.* **2020**, *120* (20), 11194−11294.

(3) Zhou, H.; Yi, X.; Hui, Y.; Wang, L.; Chen, W.; Qin, Y.; Wang, M.; Ma, J.; Chu, X.; Wang, Y.; Hong, X.; Chen, Z.; Meng, X.; Wang, H.; Zhu, Q.; Song, L.; Zheng, A.; Xiao, F. S. Isolated boron in zeolite for oxidative dehydrogenation of propane. *Science* **2021**, *372*, 76−80.

(4) Snyder, B. E. R.; Bols, M. L.; Rhoda, H. M.; Plessers, D.; Schoonheydt, R. A.; Sels, B. F.; Solomon, E. I. Cage effects control the mechanism of methane hydroxylation in zeolites. *Science* **2021**, *373*, 327−331.

(5) Liu, X.; Luo, Y.; Mao, W.; Jiang, J.; Xu, H.; Han, L.; Sun, J.; Wu, P. 3D Electron Diffraction Unravels the New Zeolite ECNU-23 from the "Pure" Powder Sample of ECNU-21. *Angew. Chem., Int. Ed.* **2020**, *59* (3), 1166−1170.

(6) Lu, K.; Huang, J.; Ren, L.; Li, C.; Guan, Y.; Hu, B.; Xu, H.; Jiang, J.; Ma, Y.; Wu, P. High Ethylene Selectivity in Methanol-to-Olefin (MTO) Reaction over MOR-Zeolite Nanosheets. *Angew. Chem., Int. Ed.* **2020**, *59* (15), 6258−6262.

(7) Sun, M. H.; Chen, L. H.; Yu, S.; Li, Y.; Zhou, X. G.; Hu, Z. Y.; Sun, Y. H.; Xu, Y.; Su, B. L. Micron-Sized Zeolite Beta Single Crystals Featuring Intracrystal Interconnected Ordered Macro-Meso-Microporosity Displaying Superior Catalytic Performance. *Angew. Chem., Int. Ed.* **2020**, *59* (44), 19582−19591.

(8) Wu, Q.; Zhu, L.; Chu, Y.; Liu, X.; Zhang, C.; Zhang, J.; Xu, H.; Xu, J.; Deng, F.; Feng, Z.; Meng, X.; Xiao, F. S. Sustainable Synthesis of Pure Silica Zeolites from a Combined Strategy of Zeolite Seeding and Alcohol Filling. *Angew. Chem., Int. Ed.* **2019**, *58* (35), 12138−12142.

(9) Xu, H.; Zhu, L.; Wu, Q.; Meng, X.; Xiao, F. S. Advances in the synthesis and application of the SSZ-39 zeolite. *Inorg. Chem. Front.* **2022**, *9* (6), 1047−1057.

(10) Li, S.; Han, L.; Zhao, Z.; Xu, H.; Jiang, J.; Wu, P. Zeolites featuring 14 × 12-ring channels with unique adsorption properties. *Inorg. Chem. Front.* **2021**, *8* (24), 5277−5285.

(11) Yu, W.; Wu, X.; Cheng, B.; Tao, T.; Min, X.; Mi, R.; Huang, Z.; Fang, M.; Liu, Y. Synthesis and Applications of SAPO-34 Molecular Sieves. *Chem. Eur. J.* **2021**, *28* (11), e202102787.

(12) Yang, M.; Fan, D.; Wei, Y.; Tian, P.; Liu, Z. Recent Progress in Methanol-to-Olefins (MTO) Catalysts. *Adv. Mater.* **2019**, *31* (50), 1902181.

(13) Zhao, D.; Zhang, Y.; Li, Z.; Wang, Y.; Yu, J. Synthesis of AEI/CHA intergrowth zeolites by dual templates and their catalytic performance for dimethyl ether to olefins. *Chem. Eng. J.* **2017**, *323*, 295−303.

(14) Gao, M.; Li, H.; Yang, M.; Zhou, J.; Yuan, X.; Tian, P.; Ye, M.; Liu, Z. A modeling study on reaction and diffusion in MTO process over SAPO-34 zeolites. *Chem. Eng. J.* **2019**, *377*, 119668.

(15) Zhou, Y.; Qi, L.; Wei, Y.; Yuan, C.; Zhang, M.; Liu, Z. Methanol-to-olefin induction reaction over SAPO-34. *Chin. J. Catal.* **2016**, *37* (9), 1496−1501.

(16) Álvaro-Muñoz, T.; Sastre, E.; Márquez-Álvarez, C. Microwave-assisted synthesis of plate-like SAPO-34 nanocrystals with increased catalyst lifetime in the methanol-to-olefin reaction. *Catal. Sci. Technol.* **2014**, *4* (12), 4330−4339.

(17) Askari, S.; Sedighi, Z.; Halladj, R. Rapid synthesis of SAPO-34 nanocatalyst by dry gel conversion method templated with morphline: Investigating the effects of experimental parameters. *Microporous Mesoporous Mater.* **2014**, *197*, 229−236.

(18) Han, D.; Yang, D.; Bi, C.; Zhang, G.; Yang, F.; Hao, Q.; Zhang, J.; Chen, H.; Ma, X. Dry-gel conversion synthesis of SAPO-14 zeolites for the selective conversion of methanol to propylene. *Inorg. Chem. Front.* **2023**, *10* (21), 6193−6203.

(19) Chang, N.; Bai, L.; Zhang, Y.; Zeng, G. Fast synthesis of hierarchical CHA/AEI intergrowth zeolite with ammonium salts as mineralizing agent and its application for MTO process. *Chemical Papers* **2019**, *73* (1), 221−237.

(20) Askari, S.; Halladj, R. Ultrasonic pretreatment for hydrothermal synthesis of SAPO-34 nanocrystals. *Ultrason Sonochem* **2012**, *19* (3), 554−559.

(21) Sun, Q.; Xie, Z.; Yu, J. The state-of-the-art synthetic strategies for SAPO-34 zeolite catalysts in methanol-to-olefin conversion. *Nat. Sci. Rev.* **2018**, *5* (4), 542−558.

(22) Wang, X.; Ma, Y.; Wu, Q.; Wen, Y.; Xiao, F.-S. Zeolite nanosheets for catalysis. *Chem. Soc. Rev.* **2022**, *51* (7), 2431−2443.

(23) Shen, B.; Chen, X.; Fan, X.; Xiong, H.; Wang, H.; Qian, W.; Wang, Y.; Wei, F. Resolving atomic SAPO-34/18 intergrowth architectures for methanol conversion by identifying light atoms and bonds. *Nat. Commun.* **2021**, *12* (1), 2212.

(24) Sławiński, W. A.; Wragg, D. S.; Akporiaye, D.; Fjellvåg, H. Intergrowth structure modelling in silicoaluminophosphate SAPO-18/34 family. *Microporous Mesoporous Mater.* **2014**, *195*, 311−318.

(25) Li, Y.; Huang, Y.; Guo, J.; Zhang, M.; Wang, D.; Wei, F.; Wang, Y. Hierarchical SAPO-34/18 zeolite with low acid site density for converting methanol to olefins. *Catal. Today* **2014**, *233*, 2−7.

(26) Smith, R. L.; Svelle, S.; del Campo, P.; Fuglerud, T.; Arstad, B.; Lind, A.; Chavan, S.; Attfield, M. P.; Akporiaye, D.; Anderson, M. W. CHA/AEI intergrowth materials as catalysts for the Methanol-to-Olefins process. *Appl. Catal. A. Gen.* **2015**, *505*, 1−7.

(27) Liu, G.; Tian, P.; Liu, Z. Synthesis of SAPO-34 Molecular Sieves Templated with Diethylamine and Their Properties Compared with Other Templates. *Chin. J. Catal.* **2012**, *33* (1), 174−182.

(28) Masoumi, S.; Towfighi, J.; Mohamadalizadeh, A.; Kooshki, Z.; Rahimi, K. Tri-templates synthesis of SAPO-34 and its performance in MTO reaction by statistical design of experiments. *Appl. Catal. A-gen.* **2015**, *493*, 103−111.

(29) Venna, S. R.; Carreon, M. A. Synthesis of SAPO-34 crystals in the presence of crystal growth inhibitors. *J. Phys. Chem. B* **2008**, *112* (51), 16261−16265.

(30) Chen, G.; Sun, Q.; Yu, J. Nanoseed-assisted synthesis of nano-sized SAPO-34 zeolites using morpholine as the sole template with superior MTO performance. *Chem. Commun.* **2017**, *53* (100), 13328−13331.

(31) Sun, Q.; Wang, N.; Bai, R.; Chen, X.; Yu, J. Seeding induced nano-sized hierarchical SAPO-34 zeolites: cost-effective synthesis and superior MTO performance. *J. Mater. Chem. A* **2016**, *4* (39), 14978−14982.

(32) Yang, M.; Tian, P.; Wang, C.; Yuan, Y.; Yang, Y.; Xu, S.; He, Y.; Liu, Z. A top-down approach to prepare silicoaluminophosphate molecular sieve nanocrystals with improved catalytic activity. *Chem. Commun.* **2014**, *50* (15), 1845−1847.

(33) Soheili, S.; Nakhaei Pour, A.; Mohammadi, A. SAPO-34 synthesis by combinations of structure-directing agents: Experimental and Monte Carlo simulations studies. *Microporous Mesoporous Mater.* **2021**, *317*, 111003.

(34) Zhang, X.; Yang, M.; Wang, Y.; Lou, C.; Xu, S.; Tian, P.; Liu, Z. Insights on the seed selection criteria of SAPO-34 synthesis: structural units and their chemical microenvironment. *Inorg. Chem. Front.* **2023**, *10*, 3874−3883.

(35) Ye, M.; Li, H.; Zhao, Y.; Zhang, T.; Liu, Z. Chapter Five - MTO Processes Development: The Key of Mesoscale Studies. In *Advances in Chemical Engineering*; Marin, G. B.; Li, J., Eds.; Academic Press, 2015; Vol. *47*, pp 279−335.

(36) Xi, D.; Sun, Q.; Xu, J.; Cho, M.; Cho, H. S.; Asahina, S.; Li, Y.; Deng, F.; Terasaki, O.; Yu, J. In situ growth-etching approach to the preparation of hierarchically macroporous zeolites with high MTO catalytic activity and selectivity. *J. Mater. Chem. A* **2014**, *2* (42), 17994−18004.

(37) Zhao, L.; Yang, G.; Hu, H.; Sun, Y.; Ma, Z.; Peng, P.; Ng, E.-P.; Tian, P.; Guo, H.; Svetlana, M. SAPO-34 crystals with nanosheet morphology synthesized by pyrophosphoric acid as new phosphorus source. *Microporous Mesoporous Mater.* **2022**, *333*, 111753.

(38) Buchholz, A.; Wang, W.; Xu, M.; Arnold, A.; Hunger, M. Thermal stability and dehydroxylation of Brønsted acid sites in silicoaluminophosphates H-SAPO-11, H-SAPO-18, H-SAPO-31, and H-SAPO-34 investigated by multi-nuclear solid-state NMR spectroscopy. *Microporous Mesoporous Mater.* **2002**, *56* (3), 267−278.

(39) Buchholz, A.; Wang, W.; Arnold, A.; Xu, M.; Hunger, M. Successive steps of hydration and dehydration of silicoaluminophosphates H-SAPO-34 and H-SAPO-37 investigated by in situ CF MAS NMR spectroscopy. *Microporous Mesoporous Mater.* **2003**, *57* (2), 157−168.

(40) Watanabe, Y.; Koiwai, A.; Takeuchi, H.; Hyodo, S. A.; Noda, S. Multinuclear NMR Studies on the Thermal Stability of SAPO-34. *J. Catal.* **1993**, *143* (2), 430−436.

(41) Shen, W.; Li, X.; Wei, Y.; Tian, P.; Deng, F.; Han, X.; Bao, X. A study of the acidity of SAPO-34 by solid-state NMR spectroscopy. *Microporous Mesoporous Mater.* **2012**, *158*, 19−25.

(42) Ren, S.; Liu, G.; Wu, X.; Chen, X.; Wu, M.; Zeng, G.; Liu, Z.; Sun, Y. Enhanced MTO performance over acid treated hierarchical SAPO-34. *Chin. J. Catal.* **2017**, *38* (1), 123−130.

(43) Liu, Z.; Ren, S.; Yu, X.; Chen, X.; Wang, G.; Wu, X.; Yu, G.; Qiu, M.; Yang, C.; Sun, Y. Melting-assisted solvent-free synthesis of hierarchical SAPO-34 with enhanced methanol to olefins (MTO) performance. *Catal. Sci. Technol.* **2018**, *8* (2), 423−427.

(44) Dai, W. L.; Wang, X.; Wu, G. J.; Guan, N. J.; Hunger, M.; Li, L. D. Methanol-to-Olefin Conversion on Silicoaluminophosphate Catalysts: Effect of Bronsted Acid Sites and Framework Structures. *ACS Catal.* **2011**, *1* (4), 292−299.

(45) Xu, L.; Du, A.; Wei, Y.; Meng, S.; He, Y.; Wang, Y.; Yu, Z.; Zhang, X.; Liu, Z. M. Synthesis of SAPO-34 with Rich Si(4Al) Coordination Environment in the Framework and Its Catalytic Performance in the Methanol-to-Olefins Reaction. *Chin. J. Catal.* **2008**, *29* (8), 727−732.

(46) Xing, A.; Yuan, D.; Tian, D.; Sun, Q. Controlling acidity and external surface morphology of SAPO-34 and its improved performance for methanol to olefins reaction. *Microporous Mesoporous Mater.* **2019**, *288*, 109562.

(47) Wang, D.; Mo, M.; Xu, M.; Xia, Z.; Zhao, X.; Gao, B. Synthesis of nano-sized SAPO-34 using a facile micron-meter seed processing method and their enhanced performance in methanol-to-olefin reactions. *Inorg. Chem. Front.* **2024**, *11* (5), 1596−1606.

(48) Liu, Z.; Ren, S.; Yu, X.; Chen, X.; Wang, G.; Wu, X.; Yu, G.; Qiu, M.; Yang, C.; Sun, Y. Melting-assisted solvent-free synthesis of hierarchical SAPO-34 with enhanced methanol to olefins (MTO) performance. *Catal. Sci. Technol.* **2018**, *8* (2), 423−427.

(49) Wang, Q.; Dai, W.; Dai, Y.; Pan, M.; Liu, Y.; Zhang, L.; Zheng, J.; Liu, X.; Li, R.; Ma, L.; Wang, H.; Zong, Y. Design Synthesis of Low-Silica SAPO-34 Nanocrystals by Constructing Isomorphous Core-Shell Structure: An Effective Catalyst for Improving Catalytic Performances in Methanol-to-Olefins Reaction. *ACS Appl. Mater. Interfaces* **2024**, *16* (11), 14308−14320.

(50) Liu, X.; Ren, S.; Zeng, G.; Liu, G.; Wu, P.; Wang, G.; Chen, X.; Liu, Z.; Sun, Y. Coke suppression in MTO over hierarchical SAPO-34 zeolites. *RSC Adv.* **2016**, *6* (34), 28787−28791.

(51) Sun, Q.; Wang, N.; Bai, R.; Chen, G.; Shi, Z.; Zou, Y.; Yu, J. Mesoporogen-Free Synthesis of Hierarchical SAPO-34 with Low Template Consumption and Excellent Methanol-to-Olefin Conversion. *ChemSusChem* **2018**, *11* (21), 3812−3820.

(52) Zhou, Y.; Shi, H.; Wang, B.; Chen, G.; Yi, J.; Li, J. The synthesis of SAPO-34 zeolite for an improved MTO performance: tuning the particle size and an insight into the formation mechanism. *Inorg. Chem. Front.* **2021**, *8* (9), 2315−2322.

https://doi.org/10.1021/acs.iecr.5c00386
Ind. Eng. Chem. Res. 2025, 64, 9951−9959